

TWO-DIMENSIONAL MODELING OF LASER SPALLATION DRILLING OF ROCKS

P532

Zhiyue Xu, Yuichiro Yamashita¹, and Claude B. Reed

Argonne National Laboratory, Argonne, IL 60439, USA

¹ Now with Kyushu University, Japan

Abstract

High power lasers can weaken, spall, melt and vaporize natural earth materials with thermal spallation being the most energy efficient rock removal mechanism. Laser rock spallation is a very complex phenomenon that depends on many factors. Computer numerical modeling would provide a great tool to understand the fundamental of this complex phenomenon, which is crucial to the success of its applications. Complexity of modeling laser rock spallation is due to: 1) rock is a porous media, to which traditional theories of heat transfer and rock mechanics can not be directly applied, 2) the laser rock removal process involves a variety of physical phenomena, and 3) thermophysical property data for rocks are lacking, particularly the data at elevated temperatures. In this paper, we propose a combined approach to this complex problem, that is establishing models for each of the physical phenomena based on the finite difference method (FDM), then combining them into one numerical procedure using the Constrained interpolation profile-Combined Unified Procedure (C-CUP). The transient temperature and stress distributions in dry or water-saturated rocks exposed to a laser beam are calculated. The spallation boundary and rock removal efficiency are determined. The modeling results provide a better understanding of laser rock spallation and guidelines for selecting processing parameters for fast rock removal.

Introduction

Laser rock spallation is a rock removal process that utilizes laser-induced thermal stress to fracture the rock into small fragments before melting of the rock occurs. High intensity laser energy, applied on a rock that normally has very low thermal conductivity, concentrates locally on the rock surface area and causes the local temperature to increase instantaneously. This results in a local thermal stress in subsurface that is enough to spall the rock. Previous test data shows that it is the laser rock spallation that removes reservoir rocks most energy efficiently among all laser rock removal mechanisms [1]. The advantages of the laser spallation rock removal are three-folds: (1) rock is removed by spallation, so it is most energy efficient, (2) the process is easy on beam fiber-optical cable delivery due to low required laser

power for each spalling beam, and (3) small rock debris or fragments are readily flushed out by standard well flushing method. In order to take advantage of the laser spallation, recent research and development work on applications of advanced high power lasers to drilling and completion of gas and oil wells mainly focuses on two fronts. The first is to develop a multi laser beam rock spallation technique to drill large and deep holes in rocks such as gas and oil wells with a rock removal rate higher than that of conventional rotary drilling as well as flame-jet spallation. In this approach, each laser beam spalls a hole as big as the beam spot and half beam size deep. Multiple such beams are overlapped to remove a layer of large rock area. Layer by layer, a large and deep hole is drilled [2, 3]. The second front is to develop a laser rock perforation technique for gas and oil well completion applications. Perforation of gas and oil wells requires creating a hole into a composite structure of steel casing, cement, and rock formation. Current explosive charge perforation method, while capable of creating the holes, significantly reduces permeability of the rock, and is reaching its technical limits. On the other hand, lab tests demonstrate that laser beams not only cut rocks efficiently, but also significantly increase the permeability of spalling-drilled rock [4]. An innovative laser perforation system will allow the gas and oil industry to rejuvenate injection and production rates quickly and easily.

Laser rock spallation is a very complex phenomenon that depends on many factors. Simply relying on experimental study to understand this phenomenon could be costing and time-consuming. Due to lacking of currently available techniques to quantitatively assess some of the factors, it may be impossible to study these factors by experimental means alone. Computer modeling, on other hand, can establish a virtual experiment and simulate the action of the factors that are difficult to be studied by a real experiment. Complexity of modeling laser rock interaction is due to: 1) rock is a porous media, to which the traditional theory of heat transfer and rock mechanics can not be directly applied, 2) the laser rock removal process involves variety of physical phenomena such as porous flow, elastic thermal fracture, phase change and purging gas blow, which can not be modeled in a single model,

and 3) thermalphysical property data for rocks are lack, particularly the data at elevated temperature. In this paper, we propose a combined approach to this complex problem, that is establishing models for each of the physical phenomena based on the finite difference method (FDM), then combining them into one numerical procedure using the Constrained Interpolation Profile (CIP) Combined and Unified Procedure (C-CUP) method [5 - 7]. C-CUP based on FDM is developed to simulate large deformation of materials, fragmentation, multiphase problem and fluid-structure interaction problem. With this approach, the transient temperature and stress distributions in dry or water-saturated rocks exposed to a laser beam have been calculated. The spallation boundary and rock removal energy efficiency have been determined for different laser conditions. The modeling results provide a better understanding of laser rock spallation phenomenon and most importantly, guidelines for selecting processing parameters for fast rock removal.

Mathematical modeling

In this study, we consider the laser spallation of Berea Grey sandstone by a pulsed laser beam. For simplicity, the rock is divided into small 0.5 x 0.5 mm meshes. Each mesh is assumed to be composed of quartz (SiO₂), air, aluminum oxide (Al₂O₃), and iron oxide (Fe₂O₃) with certain fraction of each content and behaves like isotropic-elastic material. The numerical model system and a schematic of an enlarge mesh are shown in Figure 1. The input laser beam spot size is 10 mm in diameter.

Stress model

The time differential thermo-elastic stress strain relation is:

$$\dot{\sigma}_{ij} = \lambda \delta_{ij} \dot{\epsilon}_{kk} + 2\mu \dot{\epsilon}_{ij} - (3\lambda + 2\mu) \alpha \dot{T} \delta_{ij} \quad (1)$$

$$\sigma(x_i, t_N) = \int_0^{t_N} \dot{\sigma}(x_i, t) dt = \sum_{n=1}^N \dot{\sigma}(x_i, Ndt) dt \quad (2)$$

Where δ_{ij} is Kronecker's delta and has the following property:

$$\delta_{ij} = \begin{cases} 1 & \text{if } i = j \\ 0 & \text{if } i \neq j \end{cases}$$

$\dot{\epsilon}_{kk}$ is the mean strain rate. The Lamé elastic constants λ and μ are related to Young's modulus E and Poisson ratio ν as follows:

$$\lambda = \frac{\nu E}{(1 + \nu)(1 - 2\nu)}; \quad \mu = \frac{E}{2(1 + \nu)}$$

Governing equations

Continuous equation:

$$\frac{\partial \rho}{\partial t} + u_i \frac{\partial \rho}{\partial x_i} = -\rho \frac{\partial u_i}{\partial x_i} \quad (3)$$

Momentum equation:

$$\frac{\partial u_i}{\partial t} + u_j \frac{\partial u_i}{\partial x_j} = -\frac{1}{\rho} \frac{\partial P}{\partial x_i} + \frac{1}{\rho} \frac{\partial \sigma_{ij}}{\partial x_j} + g_i \quad (4)$$

Energy equation:

$$\rho C_v \left(\frac{\partial T}{\partial t} + u_i \frac{\partial T}{\partial x_i} \right) = \sigma_{ij} \frac{\partial u_j}{\partial x_i} + \frac{\partial}{\partial x_i} \left(k \frac{\partial T}{\partial x_i} \right) - Q \quad (5)$$

For each mesh, rock thermal property is calculated as follows,

$$Y_{mesh} = Y_r \phi_r + Y_w \phi_w + Y_{air} (1 - \phi_w - \phi_r) \quad (6)$$

Here Y is the rock property of an arbitrary content. ϕ is the volume fraction of an arbitrary content.

C-CUP method, which is compact and low calculation cost, is employed to solve the stress and governing equations for the temperature and stress distributions in the rock spalled by a pulsed laser beam. In addition, laser spallation removal of rock was simulated by recalculating the temperature and stress distributions based on the new boundary conditions inherited from the previous time step.

Numerical results

The thermal models described above are used to calculate the distributions of temperature and stresses in Berea grey sandstone, from which the spallation boundary and spallation efficiency are determined. The calculation procedures are shown in Figure 2 and are as follows:

- (1) Initialize the content of rock. Assign the boundary conditions.
- (2) According to assigned volume fraction, calculate new thermal property at each mesh.
- (3) Calculation of advection term (left hand side of all governing equations).
- (4) Calculation of input energy at each mesh with laser irradiation. This heating term is function of both position and time.
- (5) By using Eqs. 4~6, normal and shear stress are updated. Then, the velocity and temperature, which result from previous time step, are used.
- (6) Solve Poisson equation, which is derived from momentum and continuous equations, in order to update Pressure (P).
- (7) Updating velocities and temperature from momentum equation and energy equation, respectively.
- (8) If calculation time reaches termination time, calculation finishes.

The initial properties of the materials and volume fraction of each rock content used in this simulation are listed in Table 1. The laser input parameters are listed in Table 2. The pulsed laser beam was applied to the rock as bursts. One laser

burst consists of 0.5-second laser on time and one second off time. During the 0.5-second laser on time, numbers of laser pulses applied to the rock depend on the pulse repetition rate. For example, at pulse repetition rate of 100 Hz, the rate simulated in this study, number of laser pulses applied during 0.5 seconds were 50. The rock will start spallation after being exposed to the laser beam for a certain period of time when the stresses established in the rock satisfy the spallation conditions. The time interval for rock spallation is set at 0.15 seconds. In other words, rock removal occurs by laser spallation every 0.15 seconds.

Fig. 3 shows transient behavior of rock temperature at different rock locations lased by one burst of Gaussian laser beam of 800 average power and 1 ms pulse width. In Fig.3, the position that $X=0.0$ mm and $Y=0.0$ mm agrees with center of initial laser irradiation spot. Temperatures at $X=0.0$ and 1.5 has periodic increment and decrease profile like the teeth of saw. These saw like profiles result from periodic heat input due to repetition irradiation of laser. For one laser pulse, rock warms up during first 1 millisecond and cools down during next 9 milliseconds due to both heat conduction of ambient rock and heat convection of ambient gas such as air. However, net heat input is plus so that temperature rises up as time passes. These two profiles periodically become 300°K at each rock spallation interval of 0.15 sec. This is because temperature is forced to be 300°K where stresses satisfy with spallation condition in order to simulate the spallation rock removal and introduction of fresh air to the new rock surface. The temperature of fresh air is 300°K . For the rest of rock locations that are far away from the center of the initial laser radiation spot, temperatures do not have saw like profiles. This is because thermal conductivity of rock is small so that heat transfer is bad. That is, far from the irradiation spot, the effect of high repetition irradiation of laser is dull. Fig.4 shows spatial distribution of temperature along with laser center axis. From 0.15 to 0.45 sec, rock receives laser radiation so that maximum temperature is high comparing to the rest cases.

Fig.5 shows transient behaviour of stress on y-plane in y axial direction shown in Figure 1, σ_{yy} . Like the temperature profile shown in Fig.3, the transient behaviour of σ_{yy} has saw like profiles. In addition, in the rock region, the profile of σ_{yy} almost completely agrees with that of temperature for the same region. From these results, it is concluded that the main component of σ_{yy} is thermal stress. Fig.6 shows the spatial distribution of σ_{yy} along with the laser center spot. Like the relationship shown between Fig.3 and Fig.5, The spatial distribution of σ_{yy} in Fig.6 agrees with that of Fig.4.

Fig.7 shows spallation boundary. The red region represents the rock and blue region is the laser spalled rock hole filled with air. The time intervals for the four pictures from left to right are 0.15, 0.30, 0.45, and 0.60 seconds respectively. The shape of spallation hole nearly corresponds to spatial distribution of laser profile, that is, Gaussian profile. However, heat diffusion of heat conduction based on Fourier law also has similar profile to spatial distribution of spallation hole. At this stage, it is difficult to conclude which is the dominate causation. The diameter of spallation hole nearly corresponds to that of laser radiation spot size, 10.0 mm. And the depth of the hole is 3.0 mm. This simulated depth of spalled-hole is slightly less than the actual hole depth of 4.0 mm spalled by the laser beam at same conditions shown in Figure 8. This is mainly because the simulating model does not account the additional rock removal due to the assistant purging gas and in-pore water vaporization pressure.

Fig.9 shows energy efficiencies of laser spallation under three laser parameter cases listed in Table 2. For one laser burst, the spallation efficiency of 0.45 seconds is the best among energy efficiencies for 0.15, 0.30, 0.45 and 0.6 seconds. As time passes, heat propagates from surface to deeper part of rock. The propagation of heat is faster than that of the spallation boundary. Therefore, the laser energy needed to spall the rock that had been warmed up by previous laser pulses decreases as time passes. Therefore efficiency of 0.45 seconds is better than that of 0.15 seconds or 0.3 seconds. Over 0.45 seconds or at 0.5 seconds, slightly melting of rock started resulting efficiency reduction. This is another indication that the relaxation time is needed between the laser bursts to avoid rock melting reported also in reference [2]. This implies future laser-on time for a laser burst should set at 0.45 seconds for best energy efficiency. Into the second laser burst, the energy efficiency is almost unchanged over the laser-on time due to two balance factors: less laser energy needed to spall the rock with residual heat left by previous burst and more difficult to remove the lased particle from the hole by purging gas.

Conclusions

Two dimensional model was used to simulated laser spallation rock removal of Berea grey sandstone by a pulsed laser beam. The transient and spatial distributions of temperature and stresses are calculated using the model. The spallation boundary and energy efficiency were determined. The dimension of the numerically simulated spallation hole is very close to ones of the actual laser-spalled hole under the same laser conditions. The efficiency data point out that relaxation time

between laser bursts for a same rock location is needed to avoid the melting of rock.

Nomenclature

- $\dot{}$: time derivation
 dt : time step
 t_N : time at N time step (s)
 E : Young's modulus
 g_i : acceleration of gravity (m/s^2)
 P : pressure (N/m^2)
 Q : laser heat input per unit volume (W/m^3)
 t : time (s)
 T : temperature (K)
 u_i : velocity vector (m/s)
 x_i : spatial coordinate vector (m)
 Y : arbitrary thermal properties
 α : coefficient of liner thermal expansion (1/K)
 δ_{ij} : Kronecker's delta
 ϕ : volume fraction
- κ : thermal conductivity (W/mK)
- λ : Lamé's elastic constant
- μ : Lamé's elastic constant
- ν : Poisson ratio
- ϵ_{kk} : Mean strain
- ρ : density (kg/m^3)
- σ_{ij} : Stress tensor (N/m^2)

References

1. Z. Xu, C. B. Reed and G. Konercki, B. C. Gahan, R.A. Parker, S. Batarseh, R. M. Graves, H. Figueroa, and N. Skinner, "Specific

energy for pulsed laser rock drilling," Journal of Laser Application, V.15, No. 1, 2003.

2. R. Parker, Z. Xu, C. B. Reed, and R. Graves, "Drilling large diameter holes in rocks using multiple laser beams," Proceedings of 23rd International Congress on Applications of Laser & Electro-Optics, October 13 – 16, 2003, Jacksonville, Florida.
3. Zhiyue Xu, Claude B. Reed, Richard Parker, and Ramona Graves, "Laser spallation of rocks for oil well drilling," Proceedings of 23rd International Congress on Applications of Laser & Electro-Optics, October 4-7, 2004, San Francisco, California.
4. Zhiyue Xu, Claude B. Reed, Ramona Graves, and Richard Parker, "Rock perforation by pulsed Nd:YAG laser," Proceedings of 23rd International Congress on Applications of Laser & Electro-Optics, October 4-7, 2004, San Francisco, California.
5. T. Yabe, F. Xiao, and T. Utsumi, "The constrained interpolation profile method for multiphase analysis," Journal of Computational Physics, Volume 169 Issue 2, May 2001.
6. H. Mizoe, S. Yoon, M. Josho, and T. Yabe, "Numerical simulation on snow melting phenomena by CIP method," Computer Physics Communication 135 (2001) 154 – 166.
7. T. Utsumi, T. Yabe, J. Koga, T. Aoki, M. Sekine, Y. Ogata, and E. Matsunaga, "A note on the basis set approach in the constrained interpolation profile method," Journal of Computational Physics, Volume 196 Issue 1, May 2004.

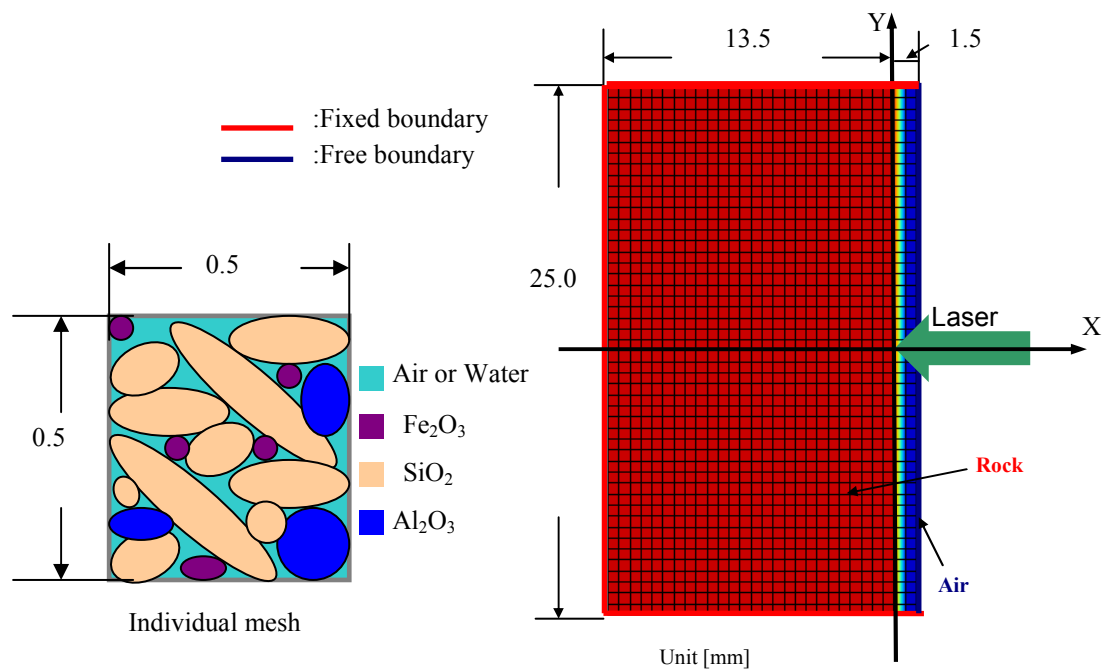


Figure 1. Numerical model used for simulating laser rock spallation (right) and detail view of an individual mesh (left).

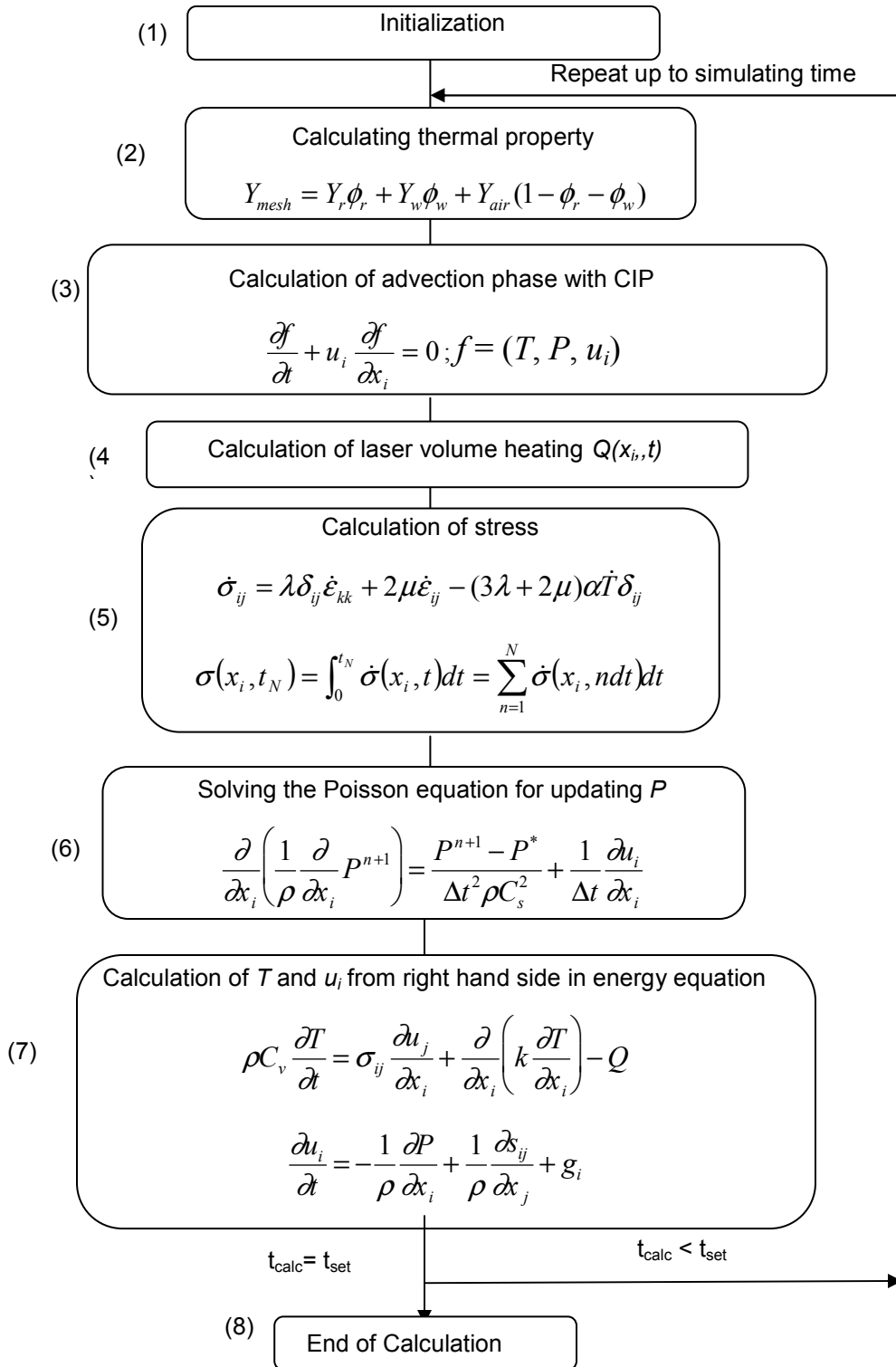


Figure 2. Flow chart showing simulation procedures

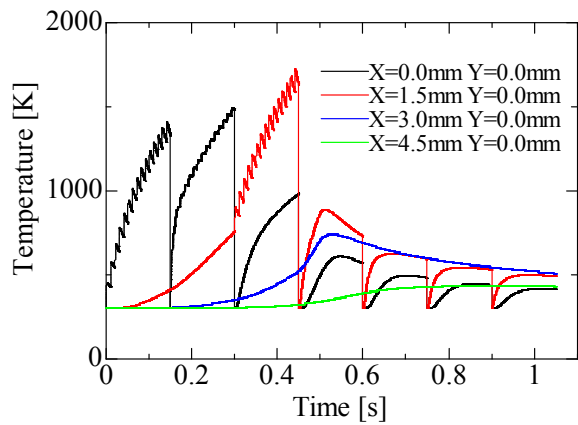


Figure 3 Transient behavior of Temperature

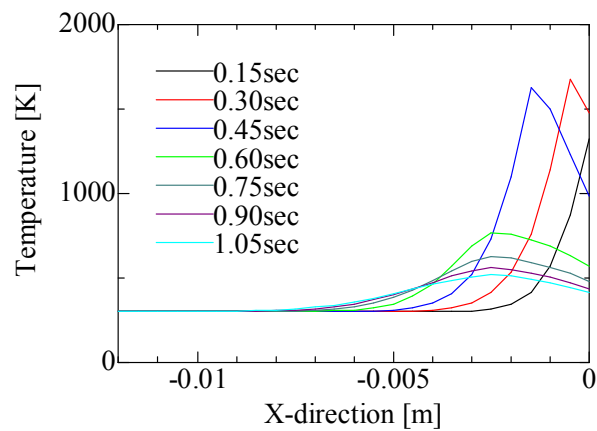


Figure 4 Spatial distribution of Temperature

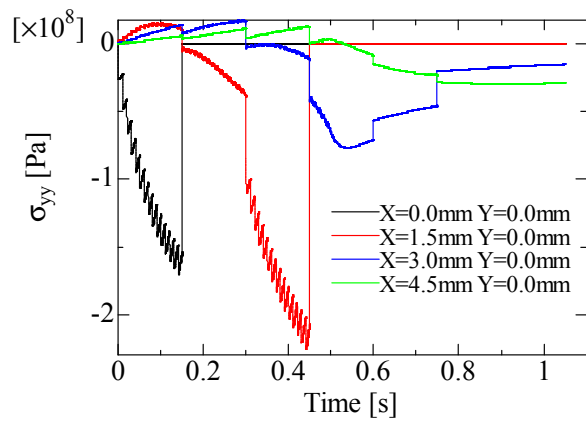


Figure 5 Transient behavior of σ_{yy}

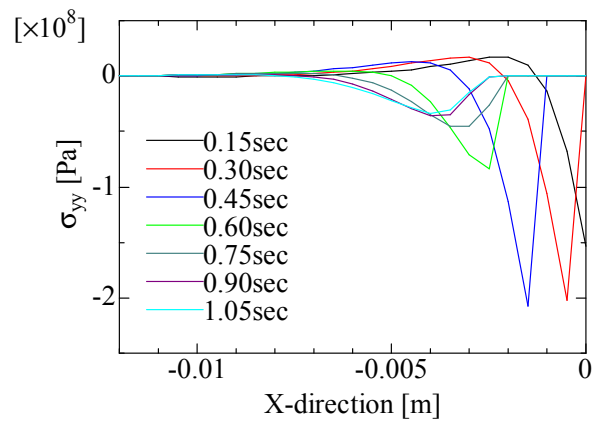


Figure 6 Spatial distribution of σ_{yy}

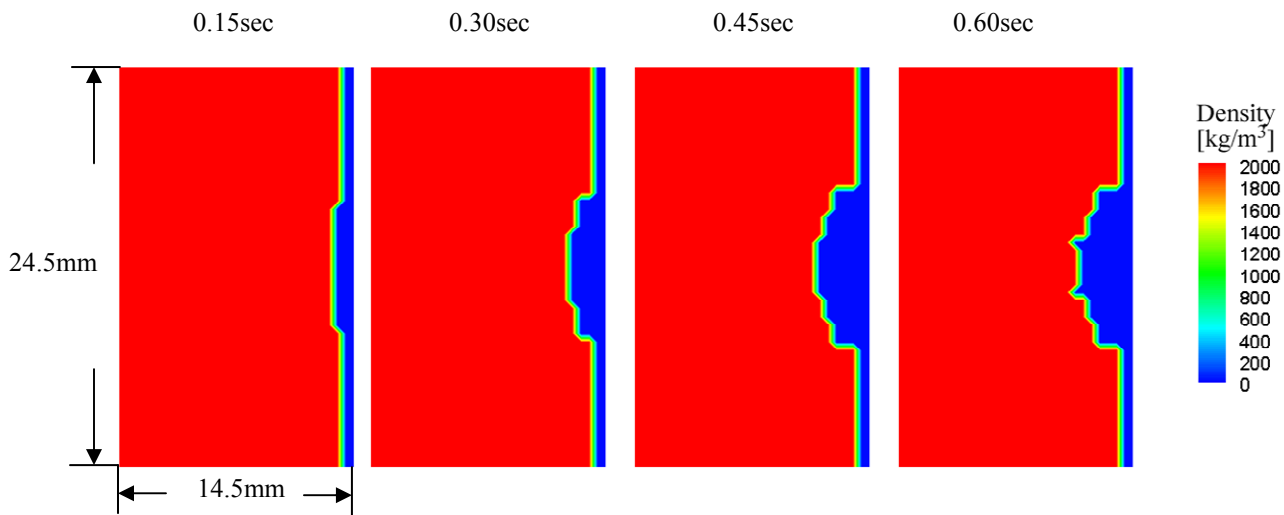


Figure 7 Spatial distribution of density

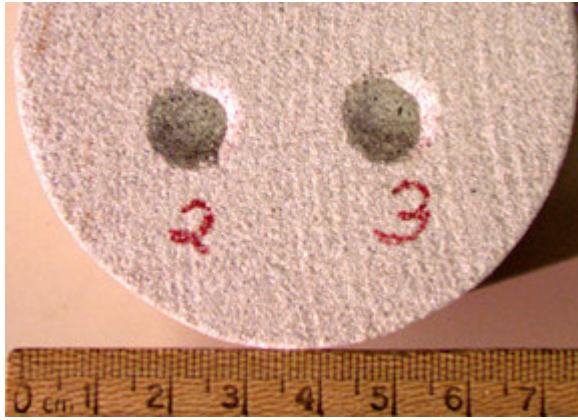


Figure 8 Two identical holes in sandstone spalled by a pulsed laser beam of 0.5 seconds at 800 W. The dimension of the holes is 10 x 4 mm.

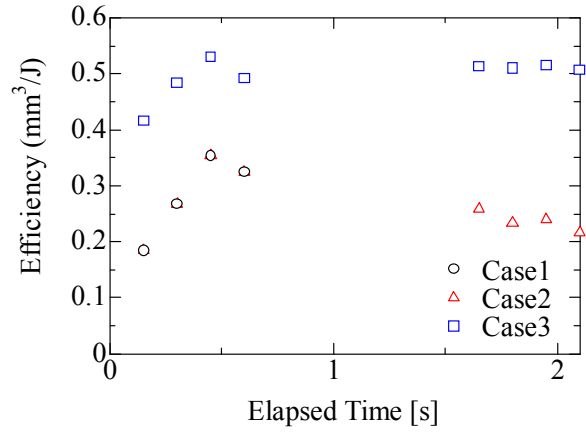


Figure 9 Energy efficiency of rock removal

Table 1. Material properties of rock contents used in the calculation

| | Silicon oxide | Aluminum oxide | Iron oxide | Air | Water | Berea gray sandstone |
|--|---------------|----------------|------------|-----------------------|------------------------|----------------------|
| Thermal conductivity [W/mK] | 1.3 – 8.2 | 25.0 | 12.5 | 2.61×10^{-3} | 0.56 | 1.8 – 2.25 |
| Specific heat capacity [J/kgK] | 733 | 800 | 627 | 717 | 4180 | 920 |
| Thermal expansion coefficient, 10^{-6} [1/K] | 10 | 10 | 10 | | | 10 |
| Density [kg/m ³] | 2650 | 7800 | 5260 | 1.16 | 998 | 2000 – 2600 |
| Volume fraction [%] | 73.95 | 0.82 | 0.20 | 25 | 25 | |
| Viscosity [Pa/s] | | | | 1.86×10^{-5} | 1.792×10^{-3} | |
| Speed of sound [m/s] | 2900 | 2900 | 2900 | 347 | 4500 | 2900 |

Table 2. Laser parameters used in the numerical modeling

| | Average power (W) | Peak power (W) | Pulse width (ms) | Pulse repetition rate (Hz) | Laser on time per burst (s) | Number of bursts | Beam profile |
|--------|-------------------|----------------|------------------|----------------------------|-----------------------------|------------------|--------------|
| Case 1 | 800 | 8000 | 1 | 100 | 0.5 | 1 | Gaussian |
| Case 2 | 800 | 8000 | 1 | 100 | 0.5 | 2 | Gaussian |
| Case 3 | 1600 | 8000 | 2 | 100 | 0.5 | 2 | Gaussian |